RSC Advances

PAPER

View Article Online
View Journal | View Issue

Cite this: *RSC Adv.*, 2014, **4**, 60842

Gels, xerogels and films of polynuclear iron(II)–aminotriazole spin-crossover polymeric complexes†

Antoni Sánchez-Ferrer,‡[a] Irene Bräunlich,‡[b] Janne Ruokolainen,[c] Matthias Bauer,[d] Rahel Schepper,[d] Paul Smith,[b] Walter Caseri*[b] and Raffaele Mezzenga*[a]

Received 9th September 2014
Accepted 6th November 2014

DOI: 10.1039/c4ra10060c

www.rsc.org/advances

The prominent polynuclear spin-crossover complex $[Fe(NH_2trz)_3](2ns)_2$ (polymer) (NH_2trz = 4-amino-1,2,4-triazole, $2ns^-$ = 2-naphthalenesulfonate) as obtained from synthesis exists in a metastable state characterized by a columnar hexagonal packing (Col_h) of polynuclear rigid–rod complexes, and shows considerable fluctuations in the spin-crossover temperature (between 22 and 41 °C upon heating and between 14 and 25 °C upon cooling). This structure is converted into a more stable columnar rectangular packing (Col_r) by annealing this material at 250 °C, which is accompanied by a shift of the spin-crossover towards higher temperatures (~52 °C upon heating and ~33 °C upon cooling). Furthermore, solutions of $[Fe(NH_2trz)_3](2ns)_2$ in dimethylformamide (DMF) can be converted into gels by increasing the concentration of $[Fe(NH_2trz)_3](2ns)_2$ or by addition of toluene, while preserving the spin-crossover behavior. Gels prepared by the latter method were converted into xerogels by CO_2 critical-point drying, or into transparent thermochromic films by slow evaporation of the solvent. For the xerogels an initial Col_h packing is transformed into the more stable Col_r packing by the same annealing procedure applied to the powders. On the other hand, the slow evaporation of solvent used for the manufacture of films allowed establishment of a Col_r packing by annealing at lower temperatures (150 °C).

Introduction

In spin-crossover complexes, the spin-state can be switched reversibly from low-spin to high-spin upon variations in temperature,[1,2] pressure,[3,4] light irradiation[5] or magnetic field.[6–8] This transition is typically accompanied by a change in various properties of the material, such as color and structure, besides, of course, magnetic susceptibility,[9–11] *i.e.* a transition from the diamagnetic to the paramagnetic state in the case of Fe^{2+} complexes.[12]

Polynuclear complexes of the type $[Fe(Rtrz)_3]_nX_{2n}$ (Rtrz = 4-R-1,2,4-triazole) have attracted particular attention, not only due to their exceptional structure but also because their spin-crossover temperature can be varied by applying differently substituted ligands and counter anions X^-.[13–15] Thus, also materials with spin-crossover near room temperature can be fabricated.[16–18]

Unfortunately, processing of those complexes is often hampered due to lacking solubility or thermal stability (usually, decomposition takes place prior to melting).[19] One possibility to overcome the poor solubility is to attach long side chains at the ligands or counter anions.[20–22] However, introducing large

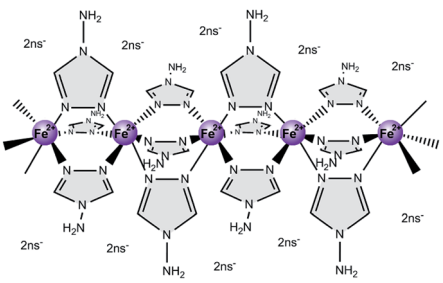

Scheme 1 Schematic representation of the structure of the spin-crossover complex $[Fe(NH_2trz)_3](2ns)_2$ (NH_2trz: 4-amino-1,2,4-triazole, $2ns^-$: 2-naphthalenesulfonate).

[a]*Department of Health Sciences and Technology, Eidgenössische Technische Hochschule (ETH) Zürich, Schmelzbergstrasse 9, 8092 Zürich, Switzerland. E-mail: raffaele.mezzenga@hest.ethz.ch; Fax: +41 44 632 16 03; Tel: +41 44 632 91 40*

[b]*Department of Materials, Eidgenössische Technische Hochschule (ETH) Zürich, Vladimir-Prelog-Weg 5, 8093 Zürich, Switzerland. E-mail: walter.caseri@mat.ethz.ch; Fax: +41 44 632 11 78; Tel: +41 44 632 22 18*

[c]*Department of Applied Physics, Aalto University School of Science, Puumiehenkuja 2, 00076 Aalto, Finland*

[d]*Fachbereich Chemie, Universität Paderborn, Warburger Straße 100, 33098 Paderborn, Germany*

† Electronic supplementary information (ESI) available: Differential scanning calorimetry (DSC) of the powders and films, wide-angle X-ray scattering (WAXS) of the gels *type B* by adding toluene after 2 or 30 min of sample preparation, polarized light microscopy (POM) of the gels *type B*, and thermogravimetric analysis (TGA) of the films. See DOI: 10.1039/c4ra10060c

‡ The first two authors contributed equally to this study.

aliphatic units reduces the relative amount of spin-crossover-active centers, *i.e.* Fe^{2+} ions and therewith attenuates the impact of the transition on the materials properties. Strikingly, one exceptional complex without side chains, $[Fe(NH_2trz)_3](2ns)_2$ ($2ns^- = 2$-naphthalene sulfonate)[16] (Scheme 1), was recently found to show good solubility in *N*,*N*-dimethylformamide (DMF).[23] Notably, the spin-crossover temperature of this polynuclear complex is close to room temperature (24 °C during heating, 10 °C during cooling) accompanied by a color change from pink (low-spin) to white (high-spin).

Processing of Fe^{2+}-triazole complexes *via* solution has been restricted hitherto to alkyl-substituted complexes, which tend to form gels in organic solvents.[21,22,24–26] Hereby the spin-crossover behavior observed in the solid state is usually retained in the gel phase,[21,25] although dependence of the transition temperature on the solvent was also reported.[24,25] When one of those gels was dried by solvent evaporation fiber-like aggregates formed, and the fibrillar structure was not fully preserved due to diffusion-crystallization phenomena.[26] Ultrathin films of amphiphilic alkyl-substituted $[Fe(Rtrz)_3]X_2$ complexes were prepared by the Langmuir–Blodgett technique.[20,21,27] However, formation of such films was limited by the instability of the complexes under aqueous conditions,[20] and only partial spin-crossover was observed in some films.[21] Moreover, a film with larger thickness exhibiting spin-crossover behavior was prepared by casting from a chloroform solution,[24] and in order to obtain a distinct spin-crossover with hysteresis, long-chain alcohol molecules had to be added to such films.

However, the alkyl-free soluble $[Fe(NH_2trz)_3](2ns)_2$ is not suitable for preparing Langmuir–Blodgett films because the complex is not amphiphilic in nature and gel-formation of $[Fe(NH_2trz)_3](2ns)_2$ in DMF, the only good solvent found so far for this complex, is expected to proceed differently than in apolar solvents used for the alkyl-substituted compounds.[23] Therefore, this study deals with the formation of $[Fe(NH_2trz)_3](2ns)_2$ spin-crossover gels under different conditions and their drying, including CO_2 critical-point drying to minimize volume shrinkage and preserve the structure. Moreover, the formation of films by solvent evaporation of the gels was studied as an alternative route for casting of solutions. The structure and thermal behavior of the different obtained solids was investigated in detail, as well as that of $[Fe(NH_2trz)_3](2ns)_2$ powders for comparison. Therefore, we present three different morphologies for the polynuclear iron(II)–aminotriazole complex, *i.e.* gel, xerogel and film state, showing the spin crossover transition temperature in the range from 29 to 40 °C – depending on the nature of the solid state –, and with a columnar packing of the linear stiff rods.

Experimental

General

Sodium 2-naphthalene sulfonate (Na(2ns)) was purchased from Alfa Aesar GmbH (Karlsruhe, Germany), iron(II) chloride tetrahydrate and 4-amino-1,2,4-triazole (NH_2trz) from Merck Chemicals (Zug, Switzerland), L-ascorbic acid from Hänseler AG (Herisau, Switzerland) and *N*,*N*-dimethylformamide from Sigma-Aldrich (Buchs, Switzerland). The syntheses of $[Fe(H_2O)_6](2ns)_2$ and $[Fe(NH_2trz)_3]_n(2ns)_{2n}$ were carried out as described earlier.[23]

Heat treatment of $[Fe(NH_2trz)_3](2ns)_2 \cdot xH_2O$

$[Fe(NH_2trz)_3](2ns)_2 \cdot xH_2O$ was heated to 250 °C under nitrogen atmosphere (at an approximate heating rate of 10 °C min^{-1}) and kept at this temperature for 5 min. Thereafter, the samples were allowed to cool down to room temperature. Elemental analysis: C 42.08% (42.20%), H 3.73% (3.81%), N 22.58% (22.70%); the calculated values are for the values with one water molecule per formula unit. Mid-infrared spectroscopy: 677 (s), 748 (s), 818 (s), 863 (m), 903 (w), 997 (w), 1032 (s), 1136 (w), 1183 (s), 1346 (m), 1385 (w), 1504 (m), 1545 (m), 1593 (m), 1630 (m, broad), 3050–3290 (s, broad), 3460 (m, broad) cm^{-1}.

Preparation of gels *type A*

Gels denominated as *type A* were obtained when $[Fe(H_2O)_6](2ns)_2$ and NH_2trz were dissolved in DMF at high iron concentrations (c_{Fe} ~0.10 M at NH_2trz/Fe^{2+} 3 : 1) or high NH_2trz/Fe^{2+} ratios (NH_2trz/Fe^{2+} 9 : 1 at c_{Fe} ~0.02 M). In the following, the preparation of a solution with $c_{Fe} = 0.037$ M at NH_2trz/Fe^{2+} ratio of 9 : 1 is described as an example. $[Fe(H_2O)_6](2ns)_2$ (214 mg, 0.37 mmol) was dissolved in degassed DMF (5 mL) under nitrogen atmosphere and combined with a solution of NH_2trz (280 mg, 3.33 mmol) in DMF (5 mL). The viscosity of the mixture increased with time and after half an hour it was still liquid with a consistence similar to that of an oil, and after 1.5 h like honey. After 6 h the mixture was highly viscous but still flowing very slowly, while after 20 h a gel formed which did not flow anymore even if turned upside down.

Preparation of gels *type B*

Gels denominated as *type B* were obtained from gels *type* A after addition of toluene in order to remove some DMF but keeping constant the NH_2trz/Fe^{2+} ratio. In the following, the preparation of a gel *type B*, at NH_2trz/Fe^{2+} ratio of 3 : 1, is described as an example. $[Fe(H_2O)_6](2ns)_2$ (78 mg, 0.14 mmol) and 4-amino-1,2,4-triazole (34 mg, 0.41 mmol) were dissolved in degassed DMF (4 mL) and stirred for 15 min. This solution was transferred into a beaker with a diameter of 3.4 cm. Subsequently, the solution was carefully covered with a layer of toluene (16 mL), and was then stored for 24 h at 3 °C. Thereafter, the top layer of solvent was removed by decantation, leaving dimensionally stable opaque gels.

Preparation of films

Gels of *type B* were slowly dried at reduced pressure (between 1 and 3 mbar) for 24 h. Transparent films with thicknesses in the order of hundreds of micrometers were thus obtained. In order to remove residual DMF (see below) the films were heated to 85 °C at 0.3 mbar for 8 h, and subsequently heated to 150 °C at 0.3 mbar.

Critical-point drying

Dried gels were prepared with a SPI-DRY CPD critical-point dryer (SPI Supplies, West Chester, USA) by the following procedure: Gels (*type B*) as described above were cut into small cubes (with an edge length of ~5 mm) and put twice into 20 mL of acetone for 15 min at room temperature. Thereafter, they were stored at −20 °C in 20 mL of acetone for at least 30 min. Subsequently, the cubes were placed into the sample chamber of the critical-point dryer and flushed 4 times with liquid CO_2 at 17–19 °C and 55 bar. After raising the temperature to 40 °C with concomitant pressure increase to 82–85 bar, CO_2 was in its supercritical state and was removed by slow release of the pressure over 6 min.

Techniques

Infrared spectra were recorded with a Bruker Vertex 70 FTIR spectrometer. Mid-infrared (MIR) spectra were recorded with a DLaTGS detector in the wavelength range of 4000 cm^{-1} to 370 cm^{-1} with samples in KBr pellets, and far-infrared (FIR) spectra with a DTGS detector between 600 cm^{-1} and 60 cm^{-1} with samples in CsI pellets. Intensities of bands are classified into weak (w), medium (m) and strong (s).

Thermogravimetric Analysis (TGA) was carried out with a TGA/SDTA851 (Mettler Toledo, Greifensee, Switzerland) instrument at a heating rate of 10 °C min^{-1} under N_2.

Differential scanning calorimetry (DSC) was performed with a Mettler DSC 822^e differential scanning calorimeter (Mettler Toledo, Greifensee, Switzerland) at a heating and cooling rate of 10 °C min^{-1} under N_2.

Elemental analyses were performed by the microanalytic laboratory of the Laboratory of Organic Chemistry (LOC), ETH Zurich.

UV/Vis spectra of solid films deposited on quartz glass were recorded with a Perkin Elmer Lambda 900 spectrometer. For variable temperature measurements a Harrick Scientific Products ATC-024-2 temperature controller equipped with a temperature controlled demountable TFC-S25 flow cell was used. Spectra were taken between 25 °C and 70 °C in steps of 5 °C. UV/Vis spectra of solutions at variable temperature were recorded with a temperature-controlled JASCO V-670 Spectrometer. Spectra were taken between −10 °C and 60 °C in steps of 5 °C. For both, solids and solutions, spectra were taken in a wavelength region of 400 nm to 800 nm and the sample was held for 3 min at the respective temperature before starting the experiment.

Samples for scanning electron microscopy (SEM) were prepared by freezing in liquid nitrogen and subsequent fracturing. Those were coated with a thin conductive layer of platinum and imaged using a LEO 1530 Gemini scanning electron microscope (LEO Elektronenmikroskopie GmbH, Oberkochen, Germany).

Polarized Optical Microscopy (POM) pictures were taken under crossed polarizers in transmission mode on a Zeiss Axioskop 2 MOT light microscope equipped with a color chilled Hamamatsu Photonics 5810 3CCD video camera.

X-ray absorption spectroscopy measurements were performed at beamline A1, Hasylab (Hamburg) as described previously.[22]

Small and wide-angle X-ray scattering (SAXS and WAXS) experiments were performed using a Rigaku MicroMax-002+ microfocused beam (40 W, 45 kV, 0.88 mA) with the $\lambda_{CuK\alpha}$ = 0.15418 nm radiation in order to obtain direct information on the scattering patterns. The scattering intensities were collected by a Fujifilm BAS-MS 2025 imaging plate system (15.2 cm × 15.2 cm, 50 μm resolution) and a 2D Triton-200 X-ray detector (20 cm diameter, 200 μm resolution). An effective scattering vector range of 0.05 $nm^{-1} < q < 25$ nm^{-1} was obtained, where q is the scattering wave vector defined as $q = 4\pi \sin\theta/\lambda_{CuK\alpha}$ with a scattering angle of 2θ. Viscous liquid and gel samples were placed in a self-constructed reusable capillary, and the scattering background was subtracted. Temperature for samples in capillaries was controlled by a homemade heating block connected to a F25-MC Julabo thermostat. Solid samples were placed in a Linkam THMS600 hot stage holder where temperature was controlled by a Linkam TMS94 temperature controller.

For transmission electron microscopy (TEM) investigations, samples were embedded in an epoxy resin at room temperature (Struers SpeciFix), and thin sections (~70 nm) were cut at −40 °C with a Leica EM UC7 microtome using a 25° Diatome diamond knife. The sections were collected on 300 mesh lacey carbon grids; no staining was used. The investigations were carried out using a Jeol JEM-3200FSC field emission microscope operating at 300 kV voltage. The images were taken in bright field mode, using zero loss energy filtering (omega type) with a slit width of 20 eV. Micrographs were recorded using a Gatan Ultrascan 4000 CCD camera. The specimen temperature was maintained at −255 °C (liquid helium) during imaging.

Results & discussion

Polynuclear $[Fe(NH_2trz)_3](2ns)_2$ complexes in the solid state

The elemental analysis, thermogravimetric analysis (see Experimental section) and the thermochromism of the compound $[Fe(NH_2trz)_3](2ns)_2$ (NH_2trz: 4-amino-1,2,4-triazole, 2ns: 2-naphthalene sulfonate) prepared in this work agree with the data published by van Koningsbruggen *et al.*[16] In addition, investigations of the complex were carried out by X-ray absorption near edge structure (XANES) spectroscopy and extended X-ray absorption fine structure (EXAFS) spectroscopy[28] at the iron K-edge.[29] Evaluation of the pre-edge signal and the white line shape (first resonances after the edge jump) allows determining the spin-state of the d^6 metal ion.[30] The corresponding spectrum is shown in Fig. 1 (black curve). Thus, the low-spin state of the complex at room temperature was substantiated (*cf.* previous analysis of the dissolved state),[23] as well as the coordination sphere of the iron(II) atoms (Table 1).

The Fe–N distances (1.99 Å) and the Fe–Fe distances (3.29 Å) are in the range of those reported for low-spin complexes of iron(II)-triazole compounds.[31] Therefore, the structure of $[Fe(NH_2trz)_3](2ns)_2$ [16] is also supported by EXAFS data.

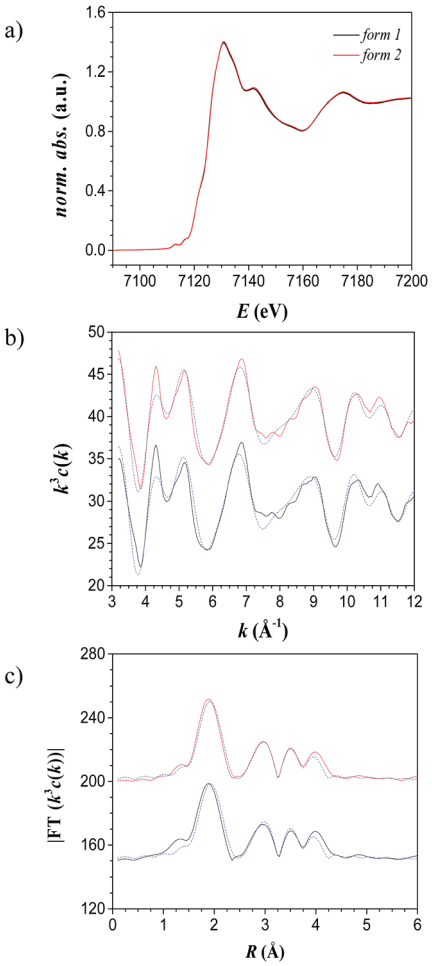

Fig. 1 X-ray absorption spectra of solid $[Fe(NH_2trz)_3](2ns)_2$ as synthesized (black line) and after annealing at 250 °C for 10 min (red line). (a) XANES (b) EXAFS (calculated spectra in blue) and (c) the corresponding Fourier-transformed functions.

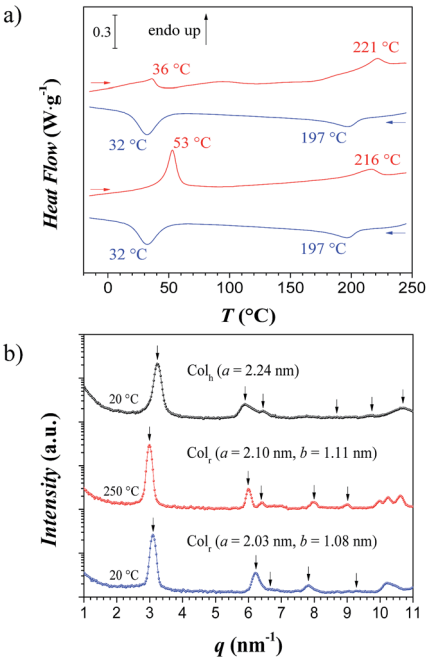

Fig. 2 (a) Differential scanning calorimetry thermograms of $[Fe(NH_2trz)_3](2ns)_2$ during 2 heating and cooling cycles (from top to bottom, first and second cycle, respectively) at heating and cooling rates of 10 °C min^{-1}. (b) WAXS 1D scattering profile for the pristine $[Fe(NH_2trz)_3](2ns)_2$ powder at 20 °C (Col_h) – black –, heating at 250 °C (Col_r) – red –, and after cooling back to 20 °C (Col_r) – blue.

According to the literature,[16] reversible spin-crossover of $[Fe(NH_2trz)_3](2ns)_2$ arises only after dehydration, with a spin-crossover temperature of 24 °C upon heating and of 10 °C upon cooling (measured by optical reflectance experiments). Dehydration is evident from an endothermic peak in differential scanning calorimetry (DSC) measurements; the end of this process was observed at about 80 °C. The dehydrated materials were characterized by spin-crossover temperatures in the range indicated in the literature.[16] However, DSC measurements of different samples revealed certain dependencies with transition temperatures from 22 to 41 °C upon heating, and from 14 to 25 °C upon cooling, although the preparation procedure was maintained identical. Moreover, aging of the samples led as well to significant fluctuations of up to 15 °C in the spin-crossover temperature. However, remarkably, when freshly synthesized $[Fe(NH_2trz)_3](2ns)_2$ was heated to 250 °C, and subsequently cooled down to room temperature, DSC revealed a shift of the spin-crossover temperature to ~53 °C

Table 1 Structural parameters of $[Fe(NH_2trz)_3](2ns)_2$ obtained by fitting the experimental EXAFS functions with theoretical models, before and after annealing at 250 °C for 10 min

Sample	*Abs-Bs*[a]	*N* (*Abs*)[b]	*R* (*Abs-Bs*)[c]/Å	σ^d/Å	E_f^e/eV (R^f/%)
$[Fe(NH_2trz)_3](2ns)_2$ as synthesized	Fe–N	6 ± 1	1.99 ± 0.02	0.08 ± 0.01	6.0
	Fe–C	12 ± 1	3.02 ± 0.03	0.09 ± 0.01	(32.2)
	Fe–Fe	2.5 ± 0.3	3.29 ± 0.03	0.11 ± 0.02	
$[Fe(NH_2trz)_3](2ns)_2$ after annealing	Fe–N	6 ± 1	1.98 ± 0.02	0.08 ± 0.01	5.9
	Fe–C	12 ± 1	3.01 ± 0.03	0.09 ± 0.01	(23.4)
	Fe–Fe	2.6 ± 0.3	3.29 ± 0.03	0.11 ± 0.02	

[a] *Abs* = X-ray absorbing atom, *Bs* = backscattering atom (neighbour). [b] Number of neighbor atoms. [c] Distance between *Abs* and *Bs*. [d] Debye–Waller like factor to account for disorder. [e] Shift between experimental and calculated spectrum. [f] Quality of the fit.

upon heating and ~32 °C upon cooling (second scan in Fig. 2a). The spin-crossover transition of the heat-treated compound was reversible since no change was found after 4 heating and cooling cycles upon removal of all residual solvent. After annealing, significantly smaller deviations of the spin-crossover temperature between the various samples were observed with values between 50 °C and 53 °C and between 30 °C and 35 °C upon heating and cooling, respectively. Notably, the optical appearance, elemental analysis and mid-infrared spectra (see Experimental section), as well as XANES and EXAFS spectra (Fig. 1, Table 1) did not differ significantly before and after annealing, indicating that the molecular short-range structure itself was preserved upon heat treatment. Hence, it appears that annealing at 250 °C transforms the as-synthesized material to a thermodynamically more stable form of $[Fe(NH_2trz)_3](2ns)_2$, suggesting that the form of the complex as synthesized is metastable. As a side remark, it should be mentioned that the stable form could not be generated by annealing the sample for 10 min at 180 °C.

In addition to the spin-crossover transitions, a transition was found by DSC at 221 °C upon heating (endothermic peak) and at 197 °C upon cooling (exothermic peak) as shown in Fig. 2a (see also Fig. ESI-1†), which is tentatively attributed to the melting of the ionic complex of the polymer with the 2-naphthalene sulfonate counter ions.

Wide angle X-ray analysis of the pristine material at 20 °C showed a Bragg peak at $q_1 = 3.24\ nm^{-1}$ together with other five peaks at q-values of 5.90, 6.31, 8.70, 9.68 and 1.07 nm^{-1} (Fig. 2b), spaced as $1 : \sqrt{3} : 2 : \sqrt{7} : 3 : \sqrt{12}$ – (10), (11), (20), (21), (30), (22) reflections – which correspond to a columnar hexagonal packing (Col_h) of the linear polynuclear complexes with a lattice parameter of $a = 2.24$ nm and a correlation length of $\xi =$ 39 nm. When heating the sample at 250 °C, a shift of the peaks towards lower q-values was observed ($q_1 = 2.99\ nm^{-1}$) due to the rearrangement of the rigid rods into a columnar rectangular packing (Col_r) with lattice parameters of $a = 2.10$ nm and $b =$ 1.11 nm, and a correlation length of $\xi = 44$ nm, as shown by the presence of the (10), (20), (11) (12) and (30) reflections; sometimes even the (01) reflection could be detected when $a \neq 2b$. Upon cooling the sample back to 20 °C, the peaks shifted towards high q-values and kept the columnar rectangular packing (Col_r) with lattice parameters of $a = 2.03$ nm and $b =$ 1.08 nm, and a correlation length of $\xi = 40$ nm. These upwards shifts indicate a contraction of the continuous phase – the 2-naphthalene sulfonate ions.

In order to substantiate the irreversible structural change established after the first heating, a second analysis was performed on an annealed sample at 250 °C (after the first heating-cooling cycle from Fig. 2a). The columnar rectangular packing (Col_r) was preserved for all temperatures. Thus, these results show the polymorphism of such linear stiff rods with a metastable columnar hexagonal packing (Col_h) below 198 °C, and a preferred columnar rectangular packing (Col_r) formed above this temperature ($\Delta H = 3$–$6\ J\ g^{-1}$) – similar to the phase transition described for organic molecules.[32]

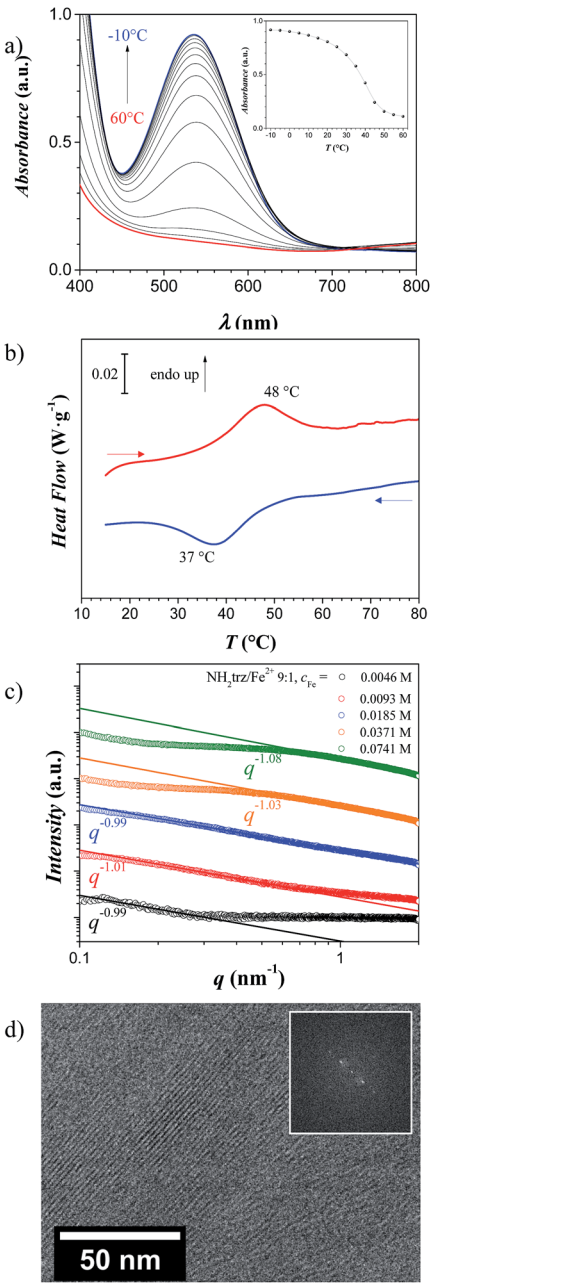

Fig. 3 (a) Temperature dependent UV/Vis spectra (between −10 °C and 60 °C in steps of 5 °C) of a $[Fe(NH_2trz)_3](2ns)_2$ gel *type A* ($c_{Fe} =$ 0.0185 M, NH_2trz/Fe^{2+} 9 : 1). The inset shows the absorbance at the absorption maximum ($\lambda = 541$ nm) as function of the temperature. (b) Differential scanning calorimetry thermograms of a $[Fe(NH_2trz)_3](2ns)_2$ gel *type A* in DMF ($c_{Fe} = 0.1$ M, NH_2trz/Fe^{2+} 3 : 1) at heating and cooling rates of 10 °C min^{-1}. (c) SAXS 1D scattering profile as function of the concentration at the constant stoichiometric ratio of NH_2trz/Fe^{2+} 9 : 1. *Note*: SAXS curves are vertically shifted for better visualization. (d) Cryo-TEM image of a gel *type A* with $c_{Fe} = 0.0741$ M and NH_2trz/Fe^{2+} 9 : 1. The inset is the Fast Fourier Transform of the cryo-TEM image.

Solutions and gels in DMF (gels *type A*)

Solutions of $[Fe(NH_2trz)_3](2ns)_2$ formed gels (in the following denoted as gels of *type A*) at higher concentrations (c_{Fe} above ~0.10 M at NH_2trz/Fe^{2+} 3 : 1) and high ligand-to-metal ratios

(NH_2trz/Fe^{2+} 9 : 1 at c_{Fe} ~0.02 M) when they were allowed to equilibrate for some time (*e.g.* about 20 h at $c_{Fe} = 0.037$ M and a NH_2trz/Fe^{2+} ratio of 9 : 1, see Experimental). Polynuclear complexes of $[Fe(NH_2trz)_3](2ns)_2$ are present as stiff, rod-like assemblies at a ligand-to-metal ratio NH_2trz/Fe^{2+} of 9 : 1.[23] In such gels, a color change upon heating to 50 °C was observed, which was also reflected in absorption measurements of visible light (Fig. 3a). Below the spin-crossover temperature, an absorption band with a maximum at 541 nm arose, which gradually disappeared during heating to elevated temperatures. The spectra revealed that this process was reversible and took place in solution in a similar temperature range as in solid state. As evident from Fig. 3a, the color change in a gel with NH_2trz/Fe^{2+} ratio of 9 : 1 ($c_{Fe} = 0.0185$ M) essentially occurred in the range between 20 °C and 45 °C. The dissolved complex at an NH_2trz/Fe^{2+} ratio of 1 : 3 was not fully established yet in DMF,[23] and thus featured a less abrupt color change at a slightly lower temperature.

Notably, upon increasing the concentration the spin-crossover temperature did not differ significantly compared to lower concentrated solutions as reflected in the DSC thermogram of a gel with $c_{Fe} = 0.10$ M and NH_2trz/Fe^{2+} 3 : 1 (Fig. 3b), where an endothermic peak at 48 °C and an exothermic peak at 37 °C were found upon heating and cooling, respectively (note that UV/vis spectra of gels were not reliable for the evaluation of the spin-crossover due to light scattering effects).

From the evaluation of the SAXS scattering profiles of solutions and gels *type A* of $[Fe(NH_2trz)_3](2ns)_2$ in DMF at different c_{Fe} from 0.0046 M to 0.0741 M, of the stoichiometric ratio of NH_2trz/Fe^{2+} 9 : 1, the formation of linear objects was confirmed by the value −1 of the slope in the scattering intensity profile, which indicates the presence of long rigid objects. Samples comprising sufficient quantities, *i.e.* at concentrations between $c_{Fe} = 0.0185$ M and 0.0741 M were gel-like (gels *type A*), and at the highest concentrations such gels showed a plateau in the middle of the scattering intensity profile, which could be attributed to the presence of a percolating network formed by these linear objects.

Cryo-TEM experiments on this gel *type A* ($c_{Fe} = 0.0741$ M and NH_2trz/Fe^{2+} 9 : 1) clearly showed the presence of such long and rigid objects with a distance of 2.0–2.1 nm between two objects and lengths up to *ca.* 100 nm (Fig. 3d), which corresponds to *ca.* 300 iron atoms per chain.

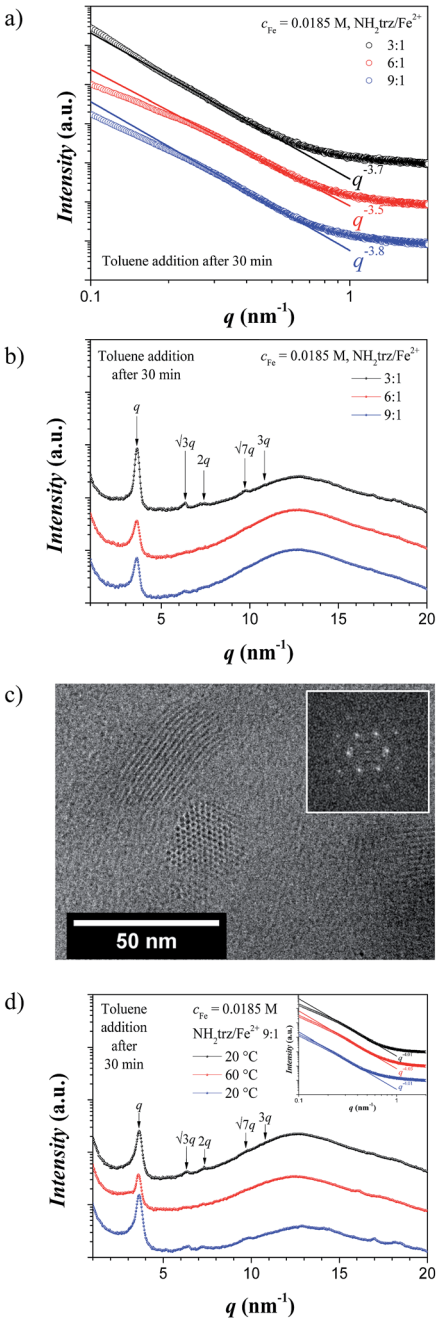

Fig. 4 (a) SAXS and (b) WAXS 1D scattering profile for the gels *type B* at constant iron concentration ($c_{Fe} = 0.0185$ M) and at different stoichiometric ratio (NH_2trz/Fe^{2+} 3 : 1, 6 : 1 and 9 : 1). (c) Cryo-TEM image of a gel *type B* at $c_{Fe} = 0.0185$ M and NH_2trz/Fe^{2+} 9 : 1 showing the columnar hexagonal packing of the rigid rods. The inset is the Fast Fourier Transform of the cryo-TEM image. (d) WAXS 1D scattering profile for a gel *type B* at constant stoichiometric ratio (NH_2trz/Fe^{2+} 9 : 1) and at constant iron concentration ($c_{Fe} = 0.0185$ M) at temperatures below (20 °C) and above (60 °C) the spin-crossover temperature. In the inset, the corresponding SAXS scattering profiles are shown. *Note*: SAXS and WAXS curves are vertically shifted for better visualization, and arrows point at expected/observed reflections for the columnar hexagonal phase.

Gels from DMF-toluene systems (gels *type B*)

When freshly prepared solutions of $[Fe(NH_2trz)_3](2ns)_2$ in DMF (c_{Fe} between 0.0185 M and 0.0741 M, and NH_2trz/Fe^{2+} between 3 : 1 to 9 : 1, note that such solutions form gels of *type* A when they are allowed to stand for hours) were carefully covered with a layer of toluene, dimensionally stable opaque gels (*type B*) formed slowly within one day due to slow diffusion of DMF to the toluene phase, which is associated with a reduction in the solubility of $[Fe(NH_2trz)_3](2ns)_2$ through effectively increasing the concentration of the polynuclear complexes in DMF. Note that at lower iron contents no gels formed (Fig. ESI-2†). SAXS analysis on these gels, designated as *type B* – addition of toluene

after 30 min of the preparation of the $[Fe(NH_2trz)_3](2ns)_2$ solution with $c_{Fe} = 0.0185$ M, and stoichiometric ratio NH_2trz/Fe^{2+} between 3 : 1 to 9 : 1 – featured slope values closed to −4 indicating the presence of sharp (Porod-like) interfaces (Fig. 4a).

As a model system, a sample with $c_{Fe} = 0.0185$ M was chosen for more detailed studies. In the WAXS region, Bragg peaks appeared with a first reflection at $q_1 = 3.63$ nm^{-1}, and additional peaks at relative positioning of $1 : \sqrt{3} : 2 : \sqrt{7} : 3$, which indicates the presence of a columnar hexagonal packing (Col_h) of the linear objects with a lattice parameter of $a = 2.00$ nm and a correlation length of $\xi = 27$ nm (Fig. 4b). Cryo-TEM images on such gels (*type B*) clearly revealed the columnar hexagonal packing of the polynuclear rods with a distance of 2.0–2.1 nm between two rigid rods and lengths of the rods up to *ca.* 60 nm (Fig. 4c), which correspond to *ca.* 180 iron atoms per polynuclear chain. More importantly, the unstained cryo-TEM images indicate that the dark cylinders correspond to the high electron density components, *i.e.* allow identifying the columns as being constituted of the iron-rich polymer backbones. The time of toluene addition after sample preparation does not seem to play any significant role as shown by the WAXS 1D scattering profile in Fig. ESI-3,† where the same structure was obtained when toluene was added 2 min after preparation of the $[Fe(NH_2trz)_3](2ns)_2$ solution. Moreover, polarized optical microscopy (POM) images confirmed the ordered nature of these gels due to the birefringence of the samples (Fig. ESI-4†).

Finally, in order to investigate the thermal stability of such gels, a sample obtained from a DMF solution with $c_{Fe} = 0.0185$ M and NH_2trz/Fe^{2+} 9 : 1 after addition of toluene was measured at 20 °C, after annealing at 60 °C – *i.e.* above the spin-crossover temperature –, and cooled back to 20 °C (Fig. 4d). The Bragg peaks at 20 °C showed again the presence of the columnar hexagonal packing of the polynuclear rods ($a = 2.00$ nm and $\xi = 25$ nm) with a small shift towards low q-values above the spin-crossover temperature ($a = 2.02$ nm and $\xi = 27$ nm), indicating that the spin-crossover did not affect the packing of the rigid rods, *i.e.* the columnar hexagonal packing of the rods did not change as confirmed from the presence of the Bragg peaks at the same position (Fig. 4d) and the same slope from the SAXS analysis (Fig. 4d inset).

Gels of *type B* showed a slightly higher spin-crossover temperature than those of *type A* where an endothermic peak at 55 °C and an exothermic peak at 42 °C were found upon heating and cooling, respectively. This shift in the spin-crossover temperature can be explained due to the removal of DMF upon addition of toluene leading to a packing of the polynuclear rods which has an effect in the electronic properties of the material.

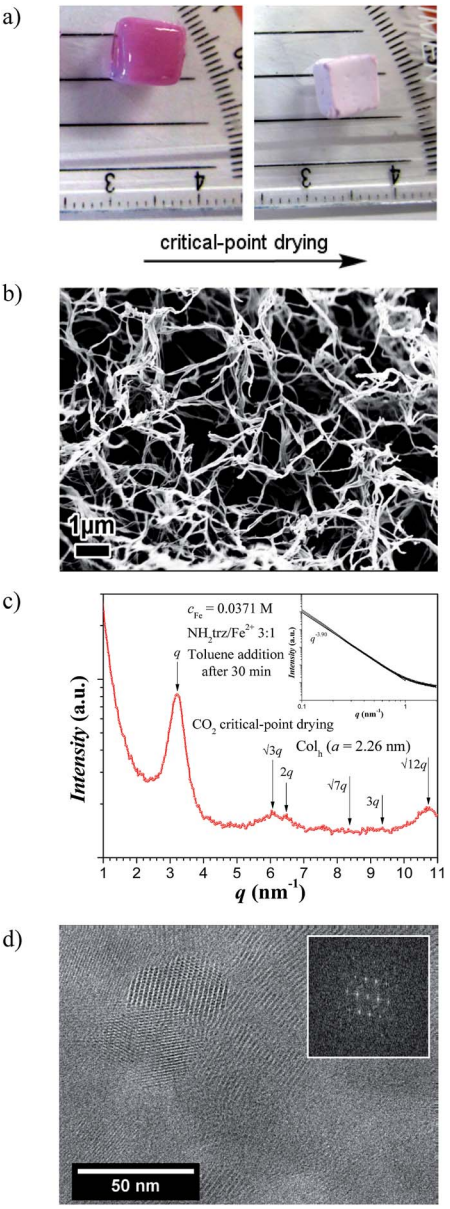

Fig. 5 (a) Photographs of a gel of *type B* at $c_{Fe} = 0.0185$ M and NH_2trz/Fe^{2+} 3 : 1 before (left) and after (right) CO_2 critical-point drying (xerogel). (b) SEM image of a dried gel at $c_{Fe} = 0.0371$ M and NH_2trz/Fe^{2+} 3 : 1 showing an open cell network. (c) WAXS 1D scattering profile of the CO_2 critical-point dried gel at $c_{Fe} = 0.0371$ M and NH_2trz/Fe^{2+} 3 : 1 showing a columnar hexagonal packing of the linear stiff rods. In the inset the corresponding SAXS scattering profile is shown. *Note*: arrows point at expected/observed reflections for the columnar hexagonal phase. (d) TEM image of the CO_2 critical-point dried gel at $c_{Fe} = 0.0371$ M and NH_2trz/Fe^{2+} 3 : 1 showing the columnar hexagonal packing of the polynuclear complexes. The inset is the Fast Fourier Transform of the cryo-TEM image.

Xerogels

Gels *type B* could be dried by the CO_2 critical-point drying technique, which allowed preserving the original shape (Fig. 5a), yet, with a shrinkage in volume amounting to ~30% of the initial volume. Scanning electron microscopy (SEM) images (Fig. 5b) of these dried gels after freeze fracturing show a loose (open cell) network with a mesh size in the micrometer range with density values between 0.02 and 0.03 g cm^{-3}.

As expected, X-ray analysis of this sample shows a slope close to −4 in the SAXS region – indicating a smooth sharp interface at these length scales–, and in the WAXS region a first peak at $q_1 = 3.21$ nm^{-1} and up to 7 higher order peaks with a relative peak

Table 2 Overview on the spin-crossover (SCO) temperature and the structural parameters of the various solids studied

Sample	SCO temperature (°C)[a]	Structural parameters[b]
Powder (pristine)	↑ 22–41 °C, ↓ 14–25 °C	Col_h, $a = 2.24$ nm, $\xi = 39$ nm
Powder (annealed at 250 °C)	↑ ~52 °C, ↓ ~33 °C	Col_r, $a = 2.03$ nm, $b = 1.08$ nm, $\xi = 39$ nm
Gel *type A* (pristine)	↑ ~48 °C, ↓ ~37 °C	Col_h, $a = 2.00$ nm
Gel *type B* (pristine)	↑ ~55 °C, ↓~42 °C	Col_h, $a = 2.00$ nm
Xerogel (pristine)	↑ ~32 °C, ↓ ~20 °C	Col_h, $a = 2.26$ nm, $\xi = 40$ nm
Xerogel (annealed at 250 °C)	↑ ~40 °C, ↓~19 °C	Col_r, $a = 2.10$ nm, $b = 1.11$, $\xi = 45$ nm
Film (dried at r.t., 1–3 mbar, with residual DMF)	↑ ~55 °C, ↓ ~50 °C	Coexistence of different structures
Film (dried at 150 °C, 0.3 mbar)	↑ ~26 °C ↓ ~10 °C	Col_r, $a = 2.01$ nm, $b = 1.08$, $\xi = 22$ nm
Film (annealed at 250 °C)	↑ ~29 °C, ↓ ~17 °C	Col_r, $a = 2.01$ nm, $b = 1.08$, $\xi = 40$ nm

[a] Temperatures according to DSC measurements: heating (↑) and cooling (↓). [b] Packing of the rods, lattice parameters and correlation length determined by WAXS.

positioning of $1 : \sqrt{3} : 2 : \sqrt{7} : 3 : \sqrt{12}$ (Fig. 5c). These results confirm the columnar hexagonal packing (Col_h) of the linear stiff rods but with a lattice parameter of $a = 2.26$ nm and a correlation length of $\xi = 16$ nm similar to that of the $[Fe(NH_2trz)_3](2ns)_2$ in the solid state. Cryo-TEM images confirm the hexagonal packing of such rigid rods in the struts of the xerogel network with a distance of 2.0–2.1 nm between two objects and lengths up to *ca.* 60 nm (Fig. 5d).

Compared to powder samples of $[Fe(NH_2trz)_3](2ns)_2$ obtained from synthesis in methanol no significant differences were found in spin-crossover behavior as long as the xerogels were kept below 80 °C. Nevertheless, slight differences in the thermal behavior were found in DSC measurements when samples were heated to 250 °C. After annealing, the spin-crossover was found to be shifted to around 40 °C upon heating, whereas a maximum at 50 °C was detected for compounds obtained from synthesis in methanol (Table 2).

X-ray analysis of the previous xerogel annealed at 250 °C showed a columnar rectangular packing (Col_r) of the rigid iron chains with lattice parameters of $a = 2.10$ nm and $b = 1.11$ nm, and a correlation length of $\xi = 45$ nm (Fig. 6a). This result is supported by cryo-TEM imaging of the sample, which identifies a distance of 2.1–2.2 nm between two neighbor rigid rods and lengths up to *ca.* 130 nm (Fig. 6b), which correspond to *ca.* 400 iron atoms per polynuclear chain.

Films

When gels of *type B* were dried by slow evaporation of the solvent at reduced pressure (see Experimental section),

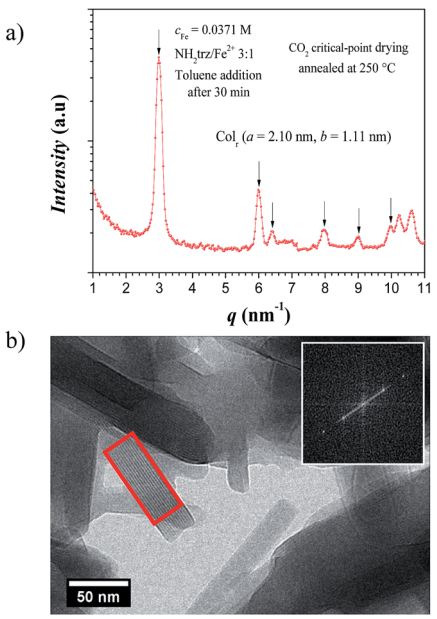

Fig. 6 (a) WAXS 1D scattering profile of the CO_2 critical-point dried gel at $c_{Fe} = 0.0371$ M and NH_2trz/Fe^{2+} 3 : 1 annealed at 250 °C showing a columnar rectangular packing of the linear stiff rods. (b) Cryo-TEM image of the annealed CO_2 critical-point drying gel at $c_{Fe} = 0.0371$ M and NH_2trz/Fe^{2+} 3 : 1. The inset is the Fast Fourier Transform of the area highlighted in red in the cryo-TEM image.

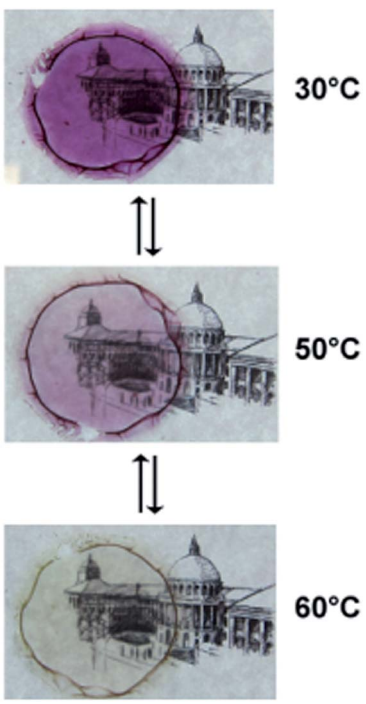

Fig. 7 Photographs of a thermochromic film of $[Fe(NH_2trz)_3](2ns)_2$ prepared from a gel of *type B* at $c_{Fe} = 0.0371$ M and NH_2trz/Fe^{2+} 3 : 1 at 30 °C, 50 °C and 60 °C.

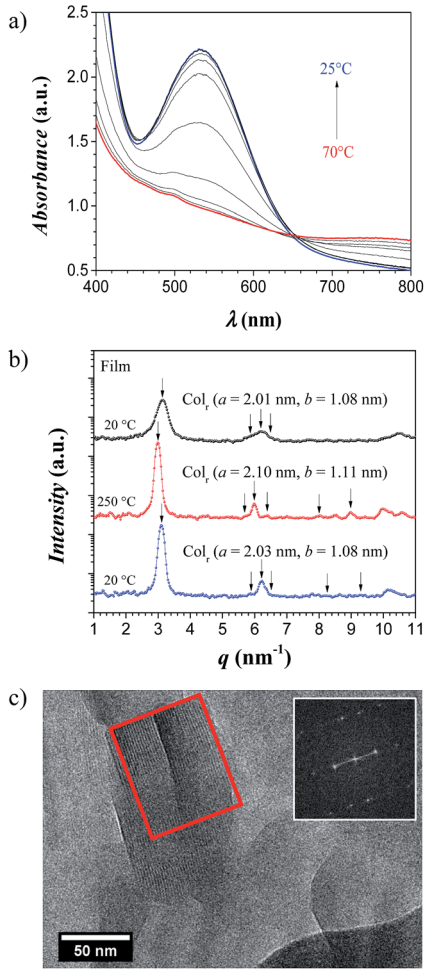

Fig. 8 (a) Temperature dependent UV/vis measurements (between 25 °C and 70 °C in steps of 5 °C) of a film with a thickness of ~240 μm. (b) WAXS 1D scattering profile for the film from a gel *type B* at $c_{Fe} = 0.0371$ M and NH_2trz/Fe^{2+} 3 : 1 at 20 °C, annealed at 250 °C, and cooled back to 20 °C, showing a columnar rectangular packing of the linear stiff rods. *Note*: arrows point at expected/observed reflections for the columnar hexagonal phase. (c) Cryo-TEM image of the film from a gel *type B* at $c_{Fe} = 0.0371$ M and NH_2trz/Fe^{2+} 3 : 1 showing the columnar rectangular packing of the polynuclear complexes. The inset is the Fast Fourier Transform of the area highlighted in red in the cryo-TEM image.

transparent thermochromic films with thicknesses in the order of 100 μm were obtained. A color change from pink to white was found at around 50 °C (Fig. 7), in agreement with the maxima in the DSC curves at ~55 °C and ~50 °C upon heating and cooling, respectively (Fig. ESI-5†). UV/vis analysis of such dried films (Fig. 8a) manifested a similar thermal behavior as solutions of $[Fe(NH_2trz)_3](2ns)_2$ in DMF. Thus, below the spin-crossover temperature the absorption band at $\lambda = 541$ nm arose upon cooling the film and disappeared after heating the sample. Such films maintained their transparency when stored for one year at ambient conditions and their thermochromic behavior was preserved. The films obtained as such, still contained about 20% w/w DMF which according to TGA diagrams was released up to a temperature of about 180 °C at ambient pressure (Fig. ESI-6†). The films dried at elevated temperature and reduced pressure (see Experimental section) showed some opacity. In addition, the spin-crossover transition evaluated by DSC shifted towards lower temperature, *i.e.* ~25 °C upon heating and ~10 °C upon cooling. Further annealing of the sample at 250 °C did not change the spin-crossover temperature to a large extent as detected by the two maxima in DSC experiments: ~29 °C upon heating and ~17 °C upon cooling (Fig. ESI-5,† Table 2).

Compared to the clear columnar hexagonal packing (Col_h) of the rods from the pristine powder after the synthesis ($a = 2.24$ nm, $\xi = 39$ nm), and the xerogel before annealing at 250 °C ($a = 2.26$ nm, $\xi = 16$ nm), the film dried *in vacuo* (1–3 mbar) and at ambient temperature showed a mixture of structures when examined with X-rays (data not shown). However, after annealing the film at 150 °C and at 0.3 mbar pressure, the sample also exhibits a columnar rectangular packing (Col_r) of the linear stiff rods with lattice parameters of $a = 2.01$ nm and $b = 1.08$ nm, and a correlation length of the rods of $\xi = 22$ nm (Fig. 8b). Upon annealing the sample at 250 °C, the columnar rectangular packing (Col_r) is preserved showing a small expansion and better correlation of the rods ($a = 2.10$ nm, $b = 1.11$ nm, and $\xi = 44$ nm). Finally, when cooling back the sample to room temperature, the lattice contracts a little bit to the initial values but maintaining high order in the domains ($a = 2.01$ nm, $b = 1.08$ nm, and $\xi = 40$ nm). Cryo-TEM image of those films

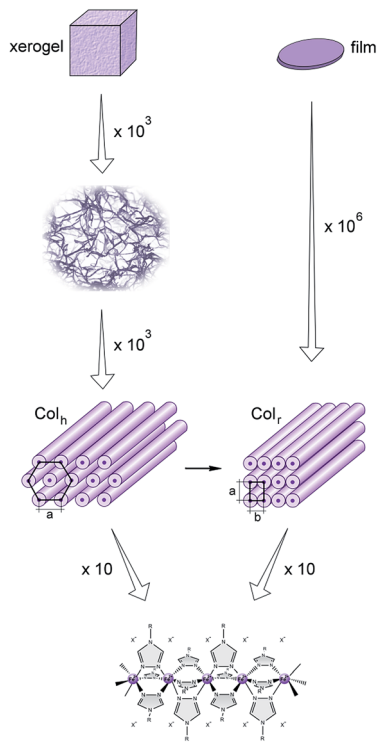

Fig. 9 Schematic representation of the xerogel and film structures at different scales, showing the columnar hexagonal packing (Col_h) of the linear stiff rods upon CO_2 critical-point drying, and the columnar rectangular packing (Col_r) of the linear stiff complexes after solvent evaporation. The Col_h crystalline structure is a metastable state which transforms towards the more stable Col_r crystalline structure.

showed two periodicities around 2.0–2.1 nm and 0.9–1.0 nm (Fig. 8c). Thus, the columnar rectangular arrangement of the linear stiff rods deduced from X-ray analysis was confirmed by TEM experiments.

The main structural findings of this study are summarised in, as a simple overview, Fig. 9, which displays a schematic representation of the structures at the different scales for both the macroscopic xerogels and films, from their mesoscale down to the molecular structure of the iron(II)-based polynuclear complex.

Conclusions

The polynuclear complex $[Fe(NH_2trz)_3](2ns)_2$ (polymer) directly obtained from synthesis in methanol adopts a metastable state in which the rod-like complexes are arranged in a columnar hexagonal packing (Col_h). Fluctuations in the spin-crossover temperature upon aging and among different samples (transition temperatures between 22 °C and 41 °C during heating, and 14 °C and 25 °C during cooling) are probably a result of the metastability. After annealing at 250 °C, a columnar rectangular packing (Col_r) was found, representing a thermodynamically more stable state featuring steady spin-crossover behavior with a transition temperature of 52 °C during heating and 33 °C during cooling. Thus, the spin-crossover temperature of this complex showed a significant dependence on the structural arrangement. An additional reversible endothermic peak observed in DSC analysis at around 220 °C might be assigned to transformation of the 2-naphthalene sulfonate counter ion into a mobile, liquid-like state which allows for the formation of a more stable rectangular packing of the stiff polynuclear complexes.

Solutions of the linear, stiff polynuclear complexes at a certain concentration of iron ($c_{Fe} \sim 0.02$ M) form gels, which can be converted to xerogels *via* CO_2 supercritical drying or to films by slow evaporation of the solvent. The open cell networks or xerogels obtained by quenching of the gel structure are constituted by connected struts of the linear rigid iron complexes in the metastable columnar hexagonal packing (Col_h) below 200 °C, or the columnar rectangular packing (Col_r) after annealing. The films are the result of the aggregation of a columnar rectangular packing of crystalline domains upon slow evaporation of the residual solvent, which enables the preferred arrangement (Col_r) of the stiff rods. Annealing at elevated temperatures appears to generate mobility of the counter ions that allows for the formation of the columnar rectangular packing (Col_r) of the polynuclear iron(II)–aminotriazole complexes. In addition, this state also forms at lower temperatures (150 °C) than in as-synthesized powders or gels upon slow evaporation of residual solvent (DMF). Gels, as well as films, show spin-crossover in the temperature range of the solids mentioned above.

Acknowledgements

We are very grateful to the responsible scientist Dr Edmund Welter at beamline A1, Hasylab (Hamburg, Germany) and to Dr Alexander Pöthig (Technische Universitat Munchen) for helpful discussions. The financial support of the Swiss National Science Foundation (No 200021-137550) is acknowledged. We also thank the COST Action CM1302 "European Network on Smart Inorganic Polymers (SIPs)" for supporting activities in the area of coordination polymers as addressed in this publication.

References

1 L. Cambi and L. Szegö, *Ber. Dtsch. Chem. Ges. B*, 1931, **64**, 2591–2598.
2 O. Roubeau, *Chem.–Eur. J.*, 2012, **18**, 15230–15244.
3 J. Jeftić and A. Hauser, *J. Phys. Chem. B*, 1997, **101**, 10262–10270.
4 H. J. Shepherd, P. Rosa, L. Vendier, N. Casati, J. F. Létard, A. Bousseksou, P. Guionneau and G. Molnár, *Phys. Chem. Chem. Phys.*, 2012, **14**, 5265–5271.
5 S. Decurtins, P. Gütlich, C. P. Köhler, H. Spierig and A. Hauser, *Chem. Phys. Lett.*, 1984, **105**, 1–4.
6 N. Nègre, C. Conséjo, M. Goiran, A. Bousseksou, F. Varret, J. P. Tuchagues, R. Barbaste, S. Akénazy and J. G. Haasnoot, *Phys. B*, 2001, **294–295**, 91–95.
7 A. Bousseksou, K. Boukheddaden, M. Goiran, C. Consejo, M. L. Boillot and J. P. Tuchagues, *Phys. Rev. B: Condens. Matter Mater. Phys.*, 2002, **65**, 172412.
8 A. Bousseksou, F. Varret, M. Goiran, K. Boukheddaden and J. P. Tuchagues, *Top. Curr. Chem.*, 2004, **235**, 65–84.
9 K. H. Sugiyarto, D. C. Craig, A. D. Rae and H. A. Goodwin, *Aust. J. Chem.*, 1994, **475**, 869–890.
10 Y. Garcia, P. J. van Koningsbruggen, E. Codjovi, R. Lapouyade, O. Kahn and L. Rabardel, *J. Mater. Chem.*, 1997, **7**, 857–858.
11 L. G. Lavrenova, O. G. Shakirova, V. N. Ikorskii, V. A. Varnek, L. A. Sheludyakova and S. V. Larionov, *Russ. J. Coord. Chem.*, 2003, **29**, 22–27.
12 J. A. Real, A. B. Gaspar and M. C. Muñoz, *Dalton Trans.*, 2005, 2062–2079.
13 G. Vos, J. G. Haasnoot, G. C. Verschoor and J. Reedijk, *Inorg. Chim. Acta*, 1985, **102**, 187–198.
14 J. Kröber, E. Codjovi, O. Kahn, F. Grolière and C. Jay, *J. Am. Chem. Soc.*, 1993, **115**, 9810–9811.
15 N. V. Bausk, S. B. Érenburg, L. N. Mazalov, L. G. Lavrenova and V. N. Ikorskii, *J. Struct. Chem.*, 1994, **35**, 509–516.
16 P. J. van Koningsbruggen, Y. Garcia, E. Codjovi, R. Lapouyade, O. Kahn, L. Fournès and L. Rabardel, *J. Mater. Chem.*, 1997, **7**, 2069–2075.
17 Y. Garcia, P. J. van Koningsbruggen, R. Lapouyade, L. Rabardel, O. Kahn, M. Wieczorek, R. Bronisz, Z. Ciunik and M. F. Rudolf, *C. R. Acad. Sci. Paris*, 1998, **1**, 523–532.
18 S. Toyazaki, Y. Murakami, T. Komatsu, N. Kojima and T. Yokoyama, *Mol. Cryst. Liq. Cryst.*, 2000, **343**, 175–180.
19 L. G. Lavrenova, N. G. Yudina, V. N. Ikorskii, V. A. Varnek, I. M. Oglazneva and S. V. Larionov, *Polyhedron*, 1995, **14**, 1333–1337.
20 F. Armand, C. Badoux, P. Bonville, A. Ruaudel-Teixier and O. Kahn, *Langmuir*, 1995, **11**, 3467–3472.
21 O. Roubeau, B. Agricole, R. Clérac and S. Ravaine, *J. Phys. Chem. B*, 2004, **108**, 15110–15116.

22 T. Fujigaya, D. L. Jiang and T. Aida, *Chem.–Asian J.*, 2007, **2**, 106–113.
23 I. Bräunlich, A. Sánchez-Ferrer, M. Bauer, R. Schepper, P. Knüsel, J. Dshemuchadse, R. Mezzenga and W. Caseri, *Inorg. Chem.*, 2014, **53**, 3546–3557.
24 K. Kuroiwa, T. Shibata, S. Sasaki, M. Ohba, A. Takahara, T. Kunitake and N. Kimizuka, *J. Polym. Sci., Part A: Polym. Chem.*, 2006, **44**, 5192–5202.
25 M. Rubio and D. López, *Eur. Polym. J.*, 2009, **45**, 3339–3346.
26 P. Grondin, O. Roubeau, M. Castro, H. Sasdaoui, A. Colin and R. Clérac, *Langmuir*, 2010, **26**, 5184–5195.
27 O. Roubeau, E. Natividad, B. Agricole and S. Ravaine, *Langmuir*, 2007, **23**, 3110–3117.
28 M. Bauer and H. Bertagnolli, in *Methods in Physical Chemistry*, Wiley-VCH Verlag GmbH & Co. KGaA, 2012, pp. 231–269.
29 M. Bauer and C. Gastl, *Phys. Chem. Chem. Phys.*, 2010, **12**, 5575–5584.
30 G. Vankó, T. Neisius, G. Molnár, F. Renz, S. Kárpáti, A. Shukla and F. M. F. de Groot, *J. Phys. Chem. B*, 2006, **110**, 11647–11653.
31 T. Yokoyama, Y. Murakami, M. Kiguchi, T. Komatsu and N. Kojima, *Phys. Rev. B: Condens. Matter Mater. Phys.*, 1998, **58**, 14238–14244.
32 M. Lehmann, M. Jahr and J. Gutmann, *J. Mater. Chem.*, 2008, **18**, 2995–3003.